JOURNAL OF SOLID STATE CHEMISTRY 109, 231–240 (1994)

Hole and Electron Doping of R_2BaNiO_5 (R = Rare Earths)

J. A. Alonso,*,[1] I. Rasines,* J. Rodríguez-Carvajal,†,§ and J. B. Torrance‡

*Instituto de Ciencia de Materiales de Madrid, C.S.I.C., Serrano 113, 28006 Madrid, Spain; †Laboratoire Leon Brillouin (CEA-CNRS), CEN Saclay, 91191 Gif-Sur Yvette Cedex, France; ‡IBM Research Division, Almaden Research Center, 650 Harry Road, San Jose, California 95120-6099; and §Institut Laue-Langevin, 156X, 38042 Grenoble Cedex, France

Received March 19, 1993, in revised form July 7, 1993; accepted July 19, 1993

Black polycrystalline samples of the composition $R_{2-x}Ca_xBaNiO_5$ (Ni-oxidized samples), with R = Y, Nd, Er, Lu, and $0.2 \leq x \leq 0.5$, have been prepared in air by solid state reaction of R_2O_3, $CaCO_3$, BaO_2, and NiO. They crystallized in the orthorhombic Nd_2BaNiO_5 structure type, space group *Immm*, that contains chains of flattened NiO_6 octahedra sharing corners along the [1 0 0] direction. X-ray and neutron powder diffraction data show that Ca^{2+} replaces R^{3+} at random, whereas the oxygen positions remain fully occupied, which induces a proportional increase in the formal oxidation state of Ni with Ca content. The unit-cell volume decreases as a result of the shrinkage of the NiO_6 octahedra. The electrical conductivity rises with Ca doping, showing a semiconductor behavior. The linearity of the log σ vs $T^{-1/4}$ plot suggests a thermally activated electron hopping conduction mechanism, by intervalence transitions between adjacent Ni^{2+}–Ni^{3+} cations. The samples can be reduced in two steps, giving oxygen-deficient compounds in which the structure is basically unchanged. After the first step all the Ni^{3+} is reduced to Ni^{2+}. The second reduction process leads to phases, greenish in color, that are thought to contain Ni in both monovalent and divalent oxidation states. The presence of Ca^{2+} in the structure seems to be essential in the stabilization of Ni^{+}. A neutron diffraction study of the compounds $Er_{2-x}Ca_xBaNiO_{5-\delta}$, prepared in a H_2/N_2 flow at 500°C, shows that the O2 axial oxygens are lost during the reduction process. This breaks the continuity of the chains of octahedra, thus hindering the intervalence transitions along the chains. The electrical conductivity is, in fact, several orders of magnitude lower than that of the corresponding Ni-oxidized samples.

INTRODUCTION

The compounds of the family R_2BaNiO_5 (R = rare earth) crystallize in two different structural types depending on the size of the R^{3+} cation. For the larger rare earths (R = Nd, Sm, Eu, Gd, Tb, Dy, Ho, Y, Er) the structure is orthorhombic, space group *Immm*, (1–7), and shows as its more interesting feature the existence of chains of flattened NiO_6 octahedra sharing corners along the a-axis direction. These octahedra contain four equivalent Ni–O equatorial bonds, perpendicular to the chain direction [1 0 0], and two much shorter Ni–O axial bonds (e.g., 1.88 Å in the Y compound) which favor Ni–O–Ni magnetic interactions along the chains. On the other hand, there are no direct Ni–O–Ni bonds between neighboring chains. When R^{3+} is diamagnetic, e.g., Y^{3+}, strong antiferromagnetic correlations along the chains exist between the Ni^{2+} magnetic moments well above RT. However, no 3-D magnetic ordering is observed at temperatures as low as 1.5 K (8). Thus Y_2BaNiO_5 can be considered as a purely one-dimensional antiferromagnetic system. The presence of a paramagnetic rare earth induces 3-D magnetic ordering at relatively high temperatures, e.g., about 30 K for the Er compound (9).

For the smaller rare earths (R = Tm, Yb, Lu), R_2BaNiO_5 are dimorphic (10, 11). Depending on the synthesis conditions they can adopt either the above described *Immm* structure or the Sm_2BaCuO_5 structure type (12–14), orthorhombic, space group *Pnma*. In the latter structure, Ni atoms are coordinated to five oxygens in a square pyramidal arrangement. The NiO_5 pyramids are isolated (there are no common oxygens) with respect to each other.

In the research for new high-temperature superconducting and related oxides there is a renewed interest in the study of low-dimensional systems containing transition metals in which an intermediate oxidation state can be induced by hole or electron doping of the metal d-bands. This interest is driven by the expectation of a better understanding of the electric or magnetic properties of these compounds. Many oxides that can be called "bidimensional," containing layers of MO_n polyhedra, have been extensively studied from this point of view, i.e., compounds with K_2NiF_4 and related structures (e.g., 15, 16), or the simplest (Sr, Ca)CuO_2 (17).

Transition metal oxides that behave as monodimensional systems are, by far, much rarer. The R_2BaNiO_5 phases, with the *Immm* structure, seem to be good candidates to study the effects of the induction of a mixed-valence state into the Ni d-bands. With this purpose in mind the hole-doped (oxidized) $R_{2-x}Ca_xBaNiO_5$ and elec-

[1] To whom correspondence should be addressed.

0022-4596/94 $6.00

tron-doped (reduced) $R_{2-x}Ca_xBaNiO_{5-\delta}$ phases have been prepared. The field of stability, the structural changes associated with doping, and the transport properties of these phases have been studied, and the results are reported in this paper.

EXPERIMENTAL

Polycrystalline samples of nominal compositions $R_{2-x}Ca_xBaNiO_5$ (R = Y, Nd, Er, Lu; $0 \leq x \leq 1$) have been prepared by solid state reaction from mixtures of analytical grade R_2O_3, $CaCO_3$, BaO_2, and NiO. They were heated in air at 800, 900, and 1000°C for 20 hr each, with intermediate regrindings, then pelletized and heated at 1200°C (Nd and Er samples), 1180°C (Y samples), or 1150°C (Lu samples) for 20 hr and cooled at 200°C hr^{-1} to 300°C in order to favor the oxygenation of the products.

Reduced $Er_{2-x}Ca_xBaNiO_{5-\delta}$ (x = 0.19, 0.34) samples were prepared by heating $Er_{2-x}Ca_xBaNiO_5$ in a H_2(5%)/N_2(95%) flow (0.5 liter min^{-1}) for 12 hr at 500°C.

X-ray powder diffraction (XRD) patterns were obtained with Cu$K\alpha$ radiation in a Siemens D-501 goniometer controlled by a DACO-MP computer, by step scanning from 10 to 100° in 2θ, in increments of 0.05° and a counting time of 4 sec each step.

The neutron diffraction diagrams of $Er_{2-x}Ca_xBaNiO_5$ (x = 0.19, 0.34) were collected in the high-resolution D2B powder diffractometer of the Institut Laue-Langevin, Grenoble. The high-intensity mode was used to collect the spectra at 295 K. The wavelength, 1.594 Å, was selected from the 533 planes of a germanium monochromator. About 8 g of sample was enclosed in a vanadium can of 8 mm diameter. The 64 counters, spaced at 2.5° intervals, were moved by steps of 0.05° in the range $8° \leq 2\theta \leq 147.5°$.

The neutron powder data of the reduced samples $Er_{2-x}Ca_xNiO_5$ (x = 0.19, 0.34) were collected at room temperature in the multidetector DN5 diffractometer at the Siloé reactor of the Centre d'Etudes Nucléaires, Grenoble. A wavelength of 1.340 Å was selected from a Cu monochromator. The 800 detectors covered a 2θ range of 80°, from $2\theta_i = 13°$. The counting time was about 8 hr, using 6 g of sample.

Both X-ray and neutron diffraction patterns were analyzed by the Rietveld (18) method, using a strongly modified version (19) of the Young–Wiles refinement program (20). A pseudo-Voigt function was chosen to generate the line shape of the diffraction peaks. In the neutron refinements, the coherent scattering lengths for Er, Ca, Ba, Ni, and O were, respectively, 8.03, 4.90, 5.25, 10.3, and 5.805 fm.

No regions were excluded in the refinements. In cases where small amounts of CaO or NiO (both with rock-salt structure) were detected in the pattern, the profile refinement of the mixture was performed. In the final run the following parameters were refined: six background coefficients, zero-point, half-width, pseudo-Voigt, and asymmetry parameters for the peak shape; scale factors, positional, thermal anisotropic factors for the metal atoms (overall for X-ray data), occupancy factors for the oxygen positions (neutron data only), and unit-cell parameters. The relative (R, Ca) occupancy factors were also refined for the oxidized Er samples from the D2B high-resolution neutron data.

The actual atomic calcium/rare earth ratio in the structure was also determined for all the samples in an indirect way from the weight losses observed by thermal analysis under reducing conditions (Equation (2) in Results, Section 3.2). Thermogravimetric (TG) curves were obtained in a Mettler TA3000 system equipped with a TG50 unit and a TC10 processor unit. Heating rates between 10 and 5° min^{-1} were used up to 950°C, in a H_2(5%)/N_2(95%) flow of 0.2 liter min^{-1}. About 50 mg of sample was used in each experiment.

Resistivity measurements have been performed by the standard d.c. four probe method between 77 and 290 K in sintered pellets with an observed density of about 85% of the theoretical crystallographic value. Infrared spectra were recorded in a Pye Unicam SP3-300S in the 200–4000 cm^{-1} range, using KBr pellets.

RESULTS

1. Composition of the Samples

The field of stability of the $R_{2-x}Ca_xBaNiO_5$ phases with *Immm* structure has been studied for R = Nd, Y, Er, Lu, and starting compositions that would lead to stoichiometries ranging from $x = 0$ to $x = 1$. The undoped ($x = 0$) Nd, Y, and Er compounds, which are well known, were also prepared for comparative purposes. The color of the $x = 0$ samples is grey and it becomes black even for the smallest Ca contents, $x \approx 0.2$. The undoped Lu_2BaNiO_5 had not been prepared yet as a pure phase in the *Immm* form (11), since the *Pnma* polymorph stabilizes under the standard ceramic preparative conditions (1150°C, 1 atm). However, $Lu_{2-x}Ca_xBaNiO_5$ crystallizes in the *Immm* structure for Ca contents $x \geq 0.18$. Probably, the mean (Lu^{3+}, Ca^{2+}) ionic size of the doped phases exceeds a "critical size" above which the *Pnma* polymorph is not thermodynamically stable.

Table 1 shows the structural Ca content for a given starting composition, together with the unit-cell parameters of the *Immm* phases present in the product. For the sake of consistency, the x values for all the samples are those determined from the thermal analysis curves. For starting mixtures of stoichiometry $(1 - s/2)(R_2O_3) \cdot s(CaO) \cdot (BaO \cdot NiO$ the actual Ca content (x) in the *Immm* phases is, in general, lower than s, and it tends to

TABLE 1
Composition and Unit-Cell Parameters of the $R_{2-x}Ca_xBaNiO_5$ Phases, for Starting Mixtures with $sCaO:(1 - s/2)R_2O_3$ Ratios

R	s	x[1]	**a** (Å)[2]	**b** (Å)	**c** (Å)
Nd	0	0	3.8268(2)	5.9272(3)	11.6510(7)
	0.2	0.15	3.8095(2)	5.9188(3)	11.6094(8)
	0.4	0.30	3.8055(2)	5.9159(3)	11.5938(8)
	0.6	0.48	3.8040(2)	5.9137(3)	11.5869(9)
Y	0	0	3.7589(2)	5.7604(3)	11.3311(6)
	0.2	0.18	3.7500(2)	5.7639(3)	11.3138(7)
	0.4	0.36	3.7416(2)	5.7662(3)	11.2967(7)
	0.6	0.50	3.7396(2)	5.7670(3)	11.2926(8)
Er	0	0	3.7493(2)	5.7369(3)	11.2853(7)
	0.2	0.19	3.7423(2)	5.7416(3)	11.2729(7)
	0.4	0.34	3.7342(2)	5.7486(3)	11.2625(8)
	0.6	0.50	3.7314(2)	5.7506(4)	11.2577(8)
Lu	0[3]	—	—	—	—
	0.2	0.18	3.7225(2)	5.6976(2)	11.1662(4)
	0.4	0.29	3.7190(2)	5.7014(2)	11.1631(4)
	0.6	0.49	3.7167(2)	5.7037(2)	11.1614(5)

[1] The Ca contents determined by thermal analysis have an estimated error of ±0.01.
[2] For the sake of consistency, the unit-cell parameters of the $x = 0$ samples have also been measured from X-ray powder diffraction data.
[3] The *Immm* polymorph of Lu_2BaNiO_5 could not be prepared as a pure phase.

reach a limit value that cannot be surpassed by further increasing of the temperature or by prolonging the thermal treatments. Thus, for starting mixtures with $s \geq 0.4$, the presence of small amounts of CaO as impurity phase can be detected by XRD. The largest Ca content achieved in well-crystallized samples is about $x = 0.5$ (for $s = 0.6$) independently of the nature of the rare-earth cation. Beyond this s value multiple phases are observed in the XRD patterns, with no further variation of the unit-cell parameters of the *Immm* phases.

2. *Structural Changes*

Figure 1 shows the unit-cell parameters variation as a function of the Ca structural content. The volume of the lattice decreases in all cases as the Ca content rises. Since the Ca^{2+} ion is slightly larger than all of the studied rare-earth cations (the Shannon (21) ionic radii are the following: Nd = 1.05, Y = 0.96, Er = 0.945, Lu = 0.919, Ca = 1.06 Å), this contraction of the lattice can only be explained by supposing that the Ca^{2+} incorporation is accompanied by an increase in the mean oxidation state of Ni, which could presumably shorten the Ni–O distances. A neutron diffraction study has permitted us to confirm this hypothesis.

Table 2 lists the structural parameters for $Er_{2-x}Ca_xBaNiO_5$ ($x = 0.19, 0.34$), determined from neutron powder diffraction data. Figure 2 shows a representation of the structure, and Fig. 3 the diffraction profiles of $Er_{1.81}Ca_{0.19}BaNiO_5$. The good agreement factors for the proposed model confirm that Ca^{2+} ions replace at random the rare-earth cations, i.e., occupying the 4(j) positions. The refinement of the relative (Er, Ca) occupancy factors on these positions for both samples leads to the compositions $(Er_{1.78(5)}Ca_{0.22(5)})$ and $(Er_{1.64(5)}Ca_{0.36(5)})$, in agreement with the values determined from thermal analysis, $x = 0.19(1)$ and $x = 0.34(1)$, respectively. Although the refinement of the occupancy factors can be considered as a more direct method to determine the Ca content of the samples, the comparatively higher standard deviations obtained by this method lead us to consider the x values determined from thermal analysis in the following discussions. The refinement of the O1 and O2 occupancy factors shows that oxygen positions are fully occupied, within the standard deviations. Therefore, in order to maintain the electroneutrality of the crystal, the mean oxidation state of Ni must increase with x, e.g., $Ni^{2.34+}$ in $Er_{1.66}Ca_{0.34}BaNiO_5$.

The rise of the formal valence of Ni leads to a contraction of the NiO_6 octahedra. Both Ni–O1 and Ni–O2 distances decrease gradually as the Ca content in the structure increases, as can be seen in Table 3. The shortening of the equatorial distances (Ni–O1) is proportionally twice as large as that of the axial bonds (Ni–O2) along the chains of octahedra. Therefore, the octahedra become more regular as the Ni valence increases.

The volume of the ErO_7 polyhedron (monocapped trigonal prism) slightly increases as a steric consequence of the partial substitution of Ca for Er. This leads to the small increase of the **b** lattice parameter with x, which is also observed for R = Y, Lu. This steric effect seems to be overcompensated for by the electrostatic contraction of NiO_6 octahedra for $R = Nd^{3+}$, which shows a smaller difference in ionic size with Ca^{2+}, giving rise to the observed decrease of **b** with x. The same overcompensation plays along the **a** and **c** directions for all the rare earths, leading to the observed decrease of these unit-cell parameters as the Ca content of the samples rises.

3. *Thermal Analysis Under Reducing Conditions*

3.1. Undoped R_2BaNiO_5 samples. The thermal behavior of R_2BaNiO_5 in a reducing H_2/N_2 flow is illustrated in Fig. 4a for R = Er. The TG curve shows a single step starting at 700°C, which corresponds to the decomposition of the sample by oxygen loss. The weight loss corresponds to 1 oxygen atom per formula. The reduction products, identified by XRD, are Er_2BaO_4 and Ni metal. This suggests that the reduction process follows the equation

$$Er_2BaNiO_5 \xrightarrow{H_2} Er_2BaO_4 + Ni + H_2O. \qquad [1]$$

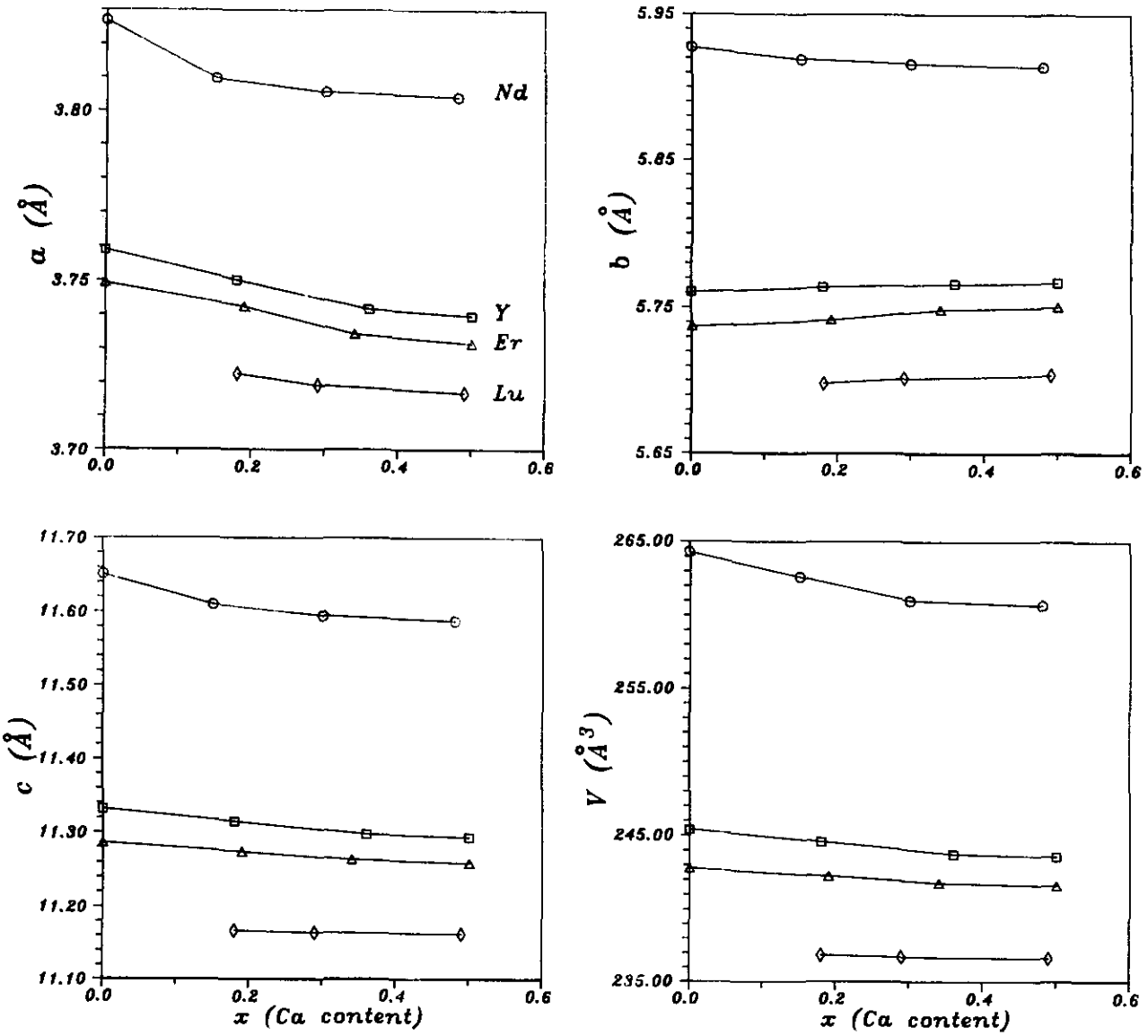

FIG. 1. Unit-cell parameters and volume variation as a function of the Ca content for $R_{2-x}Ca_xBaNiO_5$.

3.2. $R_{2-x}Ca_xBaNiO_5$ samples. Figure 4b shows a typical TG curve obtained in a H_2/N_2 flow, corresponding to R = Er, x = 0.19. A more detailed description of the thermal analysis for different rare earths and Ca contents can be found elsewhere (22). The overall thermal behavior is similar for all the samples, and can be described as follows: Three plateaux can be distinguished in the thermograms. The first one, starting between 400 and 450°C, corresponds to an initial loss of oxygen of the sample, following the equation

$$R_{2-x}Ca_xBaNiO_5 \xrightarrow{H_2} R_{2-x}Ca_xBaNiO_{5-x/2} + (x/2)H_2O. \quad [2]$$

The determination of the weight losses for this process allows us to confirm indirectly the Ca content and the Ni valence in the initial samples. After this first step, the samples are grey and the XRD patterns show that the orthorhombic *Immm* structure is conserved, with the **a** lattice parameter clearly shortened. At this point the formal oxidation state of Ni in the samples appears to be 2+.

After the first reduction, a second poorly defined process develops, whose magnitude and starting temperature strongly depend on the heating rate (22). With an isothermal heating the process can go to completion, thus avoiding the triggering of the final decomposition. The

TABLE 2
Atomic and Thermal Parameters Refined from Neutron Powder Diffraction Data at 295 K for $Er_{2-x}Ca_xBaNiO_5$

x	0	0.19	0.34
	R, Ca 4j ($\frac{1}{2}$ 0 z)		
occupancy Ca	—	0.112(24)	0.180(24)
z	0.2028(2)	0.2038(1)	0.2041(1)
B_{eq} (Å^2)	0.21(3)	0.26(3)	0.25(3)
β_{11} ($\times 10^4$)	—	75(10)	102(11)
β_{22} ($\times 10^4$)	—	16(4)	2(4)
β_{33} ($\times 10^4$)	—	6(1)	10(1)
	Ba 2c ($\frac{1}{2}$ $\frac{1}{2}$ 0)		
B_{eq} (Å^2)	0.62(7)	0.80(5)	0.80(5)
β_{11} ($\times 10^4$)	—	234(20)	271(21)
β_{22} ($\times 10^4$)	—	55(8)	46(8)
β_{33} ($\times 10^4$)	—	7(1)	4(1)
	Ni 2a (0 0 0)		
B_{eq} (Å^2)	0.29(4)	0.43(3)	0.43(3)
β_{11} ($\times 10^4$)	—	70(10)	76(10)
β_{22} ($\times 10^4$)	—	36(4)	23(5)
β_{33} ($\times 10^4$)	—	7(1)	6(1)
	O1 8l (0 y z)		
y	0.2418(5)	0.2397(3)	0.2394(3)
z	0.1487(2)	0.1481(1)	0.1472(1)
occupancy	1.0	1.01(1)	0.99(1)
B (Å^2)	0.31(4)	0.63(3)	0.59(3)
	O2 2a ($\frac{1}{2}$ 0 0)		
occupancy	1.0	1.02(1)	0.99(1)
B (Å^2)	0.45(4)	0.71(5)	0.72(6)
R factors[1]			
R_p	5.88	3.72	3.76
R_{wp}	7.52	4.68	4.78
R_{exp}	4.10	3.24	2.81
R_B	7.36	5.17	5.04

Note. Data for the $x = 0$ compound are taken from Ref (7).
[1] The discrepancy factors of the profile refinement are defined in Ref (20).

observed weight losses of this isothermal step, ideally represented in Fig. 3b, are interpreted as

$$R_{2-x}Ca_xBaNiO_{5-x/2} \xrightarrow{H_2} R_{2-x}Ca_xBaNiO_{5-x} + (x/2)H_2O. \quad [3]$$

After this step the *Immm* structure still persists; the samples are greenish and they are thought to contain Ni in a (I–II) mixed-valence state. The amount of lost oxygen corresponds exactly to the Ca content of the sample. We shall come back to this point in the Discussion.

The third plateau (starting at temperatures higher than 750°C) corresponds to the complete reduction of the material, with destruction of the *Immm* structure. The behavior is the same as that observed in the undoped samples.

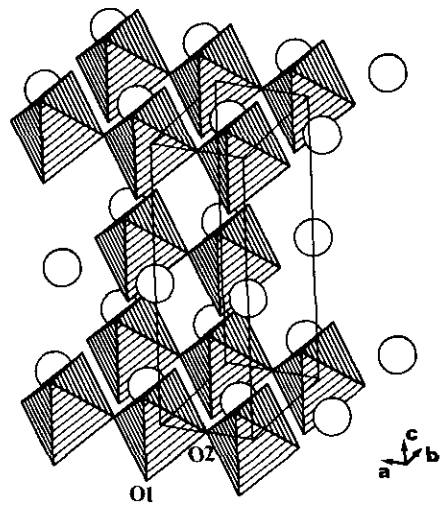

FIG. 2. Schematic view of the crystal structure of R_2BaNiO_5, outlining the chains of NiO_6 octahedra along the **a** direction. Circles correspond to Ba atoms. For the sake of clarity, R atoms are not represented.

Weight losses are those expected for complete reduction to Ni metal. The black residue at 950°C is also a mixture of a R_2BaO_4 phase (probably Ca containing) and Ni.

4. *Structural Features of the Reduced Samples*

Reduced $Er_{2-x}Ca_xBaNiO_{5-\delta}$ ($x = 0.19$, 0.34) samples were prepared by isothermal heatings in H_2/N_2 at temperatures somewhat higher than the final temperatures of the first processes observed in the TG curves. Attempts to isolate the reduced phases after the first step were unsuccessful except for the small amounts (<50 mg) which underwent short isothermal treatments (30 min) in the thermobalance. Larger samples needed for an accurate structural neutron powder diffraction study required longer isothermal treatments to get homogeneous products, which invariably led to the compositions observed after the second reduction processes. From the weight losses the oxygen deficiency of the samples was determined as $\delta = 0.21(2)$, 0.36(2) for $x = 0.19$, 0.34, respectively, which implies mean oxidation states for Ni of 1.77(4)+ and 1.62(4)+.

Table 4 shows the unit-cell and atomic parameters after the profile refinement of the powder neutron data for $Er_{2-x}Ca_xBaNiO_{5-\delta}$. Table 5 includes the most interesting interatomic distances. The **a** lattice parameter decreases strongly (1.2% for $x = 0.34$), **c** increases (0.35% for $x = 0.19$), and **b** shows no changes with respect to the Ni-oxidized samples (Ca-doped samples with five oxygens per formula). The refined occupancy factors for O1 and O2 clearly indicate that oxygen vacancies are located at the O2 positions, i.e., the axial oxygen atoms along the chains of octahedra are partially lacking. The observed

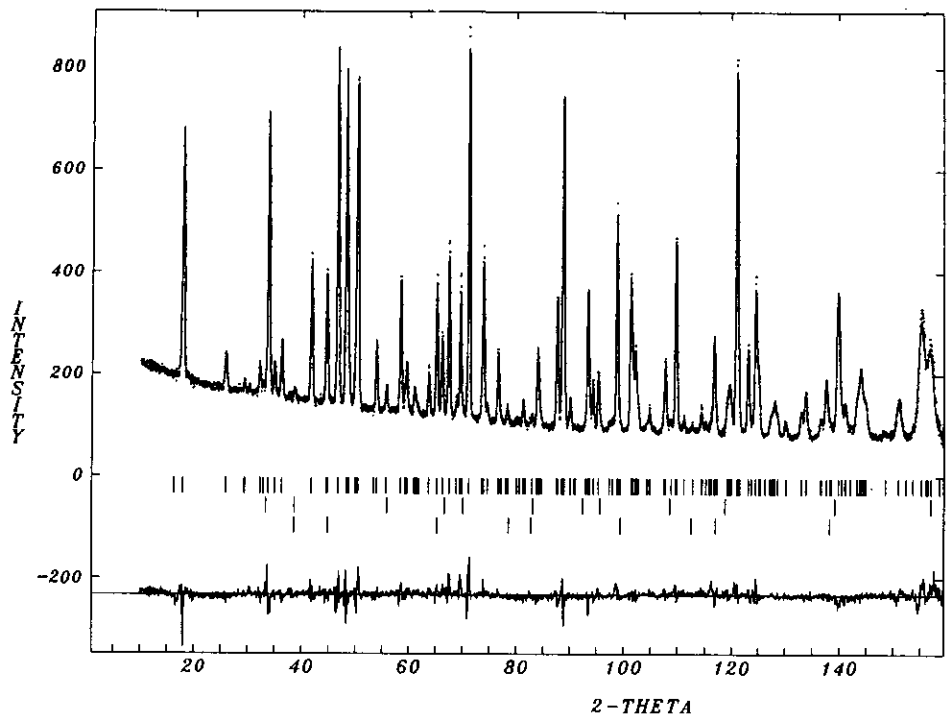

FIG. 3. Observed (crosses), calculated (solid line), and difference (at the bottom) neutron diffraction profiles for $Er_{1.81}Ca_{0.19}BaNiO_5$ at 295 K. The three series of thin marks indicate the positions of the allowed Bragg reflections for the main phase, CaO, and NiO.

shrinkage of the **a** parameter can be seen as a result of the partial collapsing of the structure along this direction. The amount of missing O2 oxygen leads to the stoichiometries $Er_{1.81}Ca_{0.19}BaNiO_{4.76(2)}$ and $Er_{1.66}Ca_{0.34}BaNiO_{4.62(2)}$ for both samples, in relatively good agreement with the values obtained from the weight losses after the reduction process.

On the other hand, Ni–O1 distances increase with respect to the oxidized samples, as a result of the average decrease of the oxidation state of Ni. The increase of the **c** parameter is related to this effect. Thermal factors for Ni are strongly anisotropic, the thermal ellipsoids being oriented along the **a** direction, which is clearly correlated with the random absence of some Ni–O2 bonds along the chains.

The (Er,Ca)O_7 polyhedra, which can be described as monocapped trigonal prisms constituted by 6O1 and 1O2, decrease in volume with regard to the oxidized samples: the absence of some O2 leads to the strengthening and shortening of the remaining (Er,Ca)–O1 distances. This is mainly due to the displacement of (Er,Ca) atoms along the [0 0 1] direction (0.01 Å in the $x = 0.34$ compound), far away from its associated O2 vacancy. As for the BaO_{10} polyhedron, which consists of 8O1 + 2O2 oxygens, Ba–O1 distances also decrease in order to compensate for the lack of some O2 oxygens. As observed for Ni, thermal factors for Ba increase greatly with respect to the Ni-oxidized samples, the flattened ellipsoids laying on the **ab** plane, which is also a consequence of the lack of some strong Ba–O2 bonds (e.g., 24% for $x = 0.19$), making the thermal vibrations of Ba easier.

It should be noted that reduced samples (containing Ni(I–II)) are unstable in air, where they slowly retake oxygen, even at room temperature.

TABLE 3
Selected Distances (Å) and Angles (°) for $Er_{2-x}Ca_xBaNiO_5$

x		0	0.19	0.34
Ni–O1	(×4)	2.180(3)	2.165(1)	2.154(1)
–O2	(×2)	1.8770(1)	1.8719(1)	1.8670(1)
(R, Ca)–O1	(×4)	2.414(2)	2.407(1)	2.407(1)
–O1	(×2)	2.240(3)	2.243(2)	2.250(2)
–O2	(×1)	2.292(2)	2.298(1)	2.297(1)
Ba–O1	(×8)	2.924(2)	2.921(1)	2.911(1)
–O2	(×2)	2.8715(1)	2.8722(1)	2.8751(1)
O1–Ni–O1		79.1(1)	79.0(1)	79.5(1)
O1–Ni–O1		100.8(2)	101.0(1)	100.5(1)

Note. Data for the $x = 0$ compound are taken from Ref (7).

5. *Resistivity Measurements*

$Er_{2-x}Ca_xBaNiO_5$ samples show a semiconducting behavior in the 77–300 K temperature range. Figure 5 shows the (log σ) vs ($T^{-1/4}$) plot for the $x = 0.0$, 0.19, 0.34

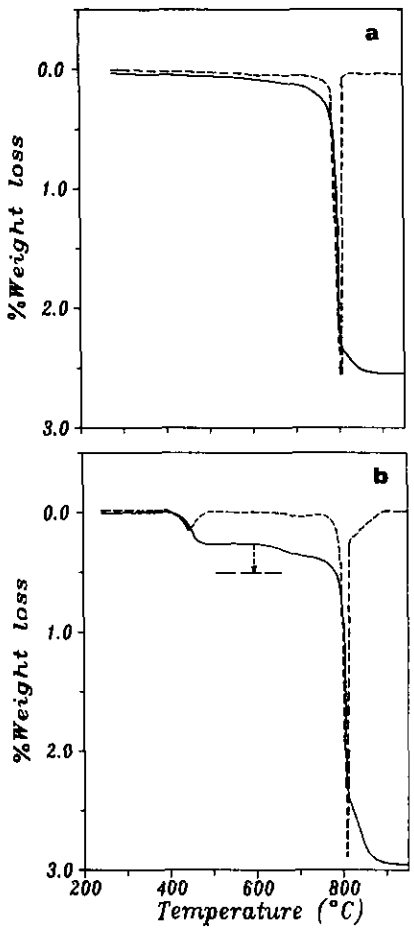

FIG. 4. TG (solid line) and DTG (broken line) curves obtained under a H_2/N_2 flow at 5° min^{-1} for (a) Er_2BaNiO_5 and (b) $Er_{1.81}Ca_{0.19}BaNiO_5$. The arrow schematically represents that a second reduction level can be reached by isothermal heating at 590°C.

TABLE 4

Unit-Cell, Atomic, and Thermal Parameters for the Reduced Samples $Er_{2-x}Ca_xBaNiO_{5-\delta}$ Refined from Neutron Powder Diffraction Data at 295 K

	x	
	0.19	0.34
a (Å)	3.7106(2)	3.6876(3)
b (Å)	5.7461(4)	5.7467(4)
c (Å)	11.3007(8)	11.3012(8)
	(*R*, Ca) 4*j* ($\frac{1}{2}$ 0 *z*)	
z	0.2047(2)	0.2049(2)
B (Å^2)	0.44(6)	0.29(10)
	Ba 2*c* ($\frac{1}{2}$ $\frac{1}{2}$ 0)	
B_{eq} (Å^2)	1.3(2)	1.3(2)
β_{11} ($\times 10^4$)	395(53)	349(53)
β_{22} ($\times 10^4$)	100(21)	71(21)
β_{33} ($\times 10^4$)	9(3)	19(3)
	Ni 2*a* (0 0 0)	
B_{eq} (Å^2)	0.9(1)	1.0(1)
β_{11} ($\times 10^4$)	482(30)	494(34)
β_{22} ($\times 10^4$)	−11(10)	12(14)
β_{33} ($\times 10^4$)	2(1)	6(2)
	O1 8*l* (0 *y z*)	
y	0.2408(6)	0.2405(6)
z	0.1487(2)	0.1476(2)
occupancy	1.01(1)	0.99(1)
B (Å^2)	0.70(8)	0.81(8)
	O2 2*b* ($\frac{1}{2}$ 0 0)	
occupancy	0.76(2)	0.62(2)
B (Å^2)	0.5(2)	0.3(2)
R factors[1]		
R_p	1.83	1.84
R_{wp}	2.56	2.57
R_{exp}	0.91	1.17
R_B	2.81	3.12

[1] The discrepancy factors of the profile refinement are defined in Ref. (20).

compounds. Room temperature conductivities are 5.8×10^{-6}, 4.2×10^{-5}, and 7.2×10^{-5} $(\Omega \cdot cm)^{-1}$, respectively. The linearity of the plots suggests that the mechanism of the electrical conductivity is the thermally activated random-range hopping of electrons between adjacent Ni^{2+}–Ni^{3+} cations. The reduced $Er_{2-x}Ca_xBaNiO_{5-\delta}$ samples show room temperature conductivities lower than 10^{-10} $(\Omega \cdot cm)^{-1}$. The variation with the temperature was not measured.

6. *Infrared Absorption Spectra*

The infrared spectra of the $x = 0$, 0.19 (oxidized) samples are shown in Fig. 6. No essential differences are observed between both diagrams, with the exception of the attenuation and shifting of the 775 cm^{-1} band ($x = 0$) toward 795 cm^{-1} ($x = 0.19$). This absorption band has been related to the stretching of the apical Ni–O2 bonds (23), the shift toward high frequencies being associated to the shortening and strengthening of these bonds as the Ni valence increases. No absorption bands are observed in either spectra in the 1200–4000 cm^{-1} region.

DISCUSSION

The black color of the $R_{2-x}Ca_xBaNiO_5$ samples and the increase of the electronic conductivity with respect to the undoped R_2BaNiO_5 samples are both related to the same fact: a mixed-valence state (II)–(III) has been induced in the Ni sublattice. The high anisotropy associated with these compounds makes it difficult to draw quantitative conclusions from the transport measurements on powder samples: the low values of the observed conductivities

TABLE 5
Selected Bond Distances (Å) and Angles (°) for the Reduced Phases $Er_{2-x}Ca_xBaNiO_{5-\delta}$

		x	
		0.19	0.34
Ni–O1	(×4)	2.177(3)	2.166(3)
–O2	(×2)	1.8555(1)	1.8441(1)
(R, Ca)–O1	(×4)	2.400(2)	2.394(2)
–O1	(×2)	2.228(3)	2.237(3)
–O2	(×2)	2.313(2)	2.316(2)
Ba–O1	(×8)	2.913(2)	2.900(2)
–O2	(×2)	2.8732(2)	2.8736(2)
O1–Ni–O1		78.9(2)	79.3(2)
O1–Ni–O1		101.1(2)	100.7(2)

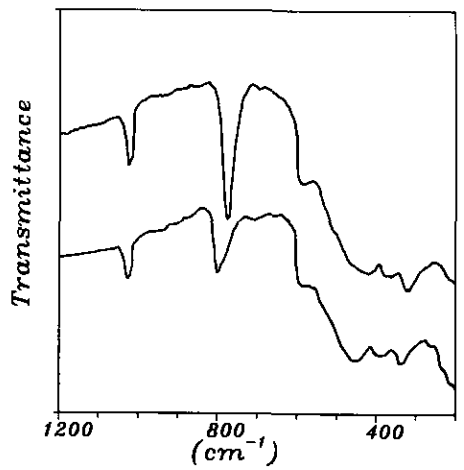

FIG. 6. Infrared spectra of $Er_{2-x}Ca_xBaNiO_5$ for $x = 0$ (upper curve) and $x = 0.19$ (lower curve).

for the relatively high levels of doping (hole concentration of 34% with respect to Ni for $x = 0.34$) suggest a poor mobility of the carriers, although this fact could partially reflect a bad electrical connectivity between adjacent microcrystals. The semiconducting behavior of the samples seems to indicate that there is no charge delocalization along the —O–Ni–O–Ni–O– chains: instead of equivalent Ni cations with a mean $2 + x$ oxidation state along each chain, it would be more precise to think about trapped Ni^{3+} cations distributed at random in a Ni^{2+} sublattice. Thus, there is an activation energy associated with the hopping of the electrons between neighboring Ni^{2+}–Ni^{3+} cations, through O2 apical oxygens. Such intervalence transitions are characteristic of mixed valence compounds in which the electrons are trapped by lattice distortions (24). In this case, Ca^{2+} cations are distributed at random in the R^{3+} sublattice, producing local distortions around which the bond lengths and strengths are slightly different. Ni atoms directly linked to Ca (through O1) are especially favored for supporting electronic holes, since Ca has a more basic character than R. Electronic holes, and therefore Ni^{3+} cations, are thus preferentially trapped in the neighborhood of Ca^{2+} cations. The local shortening of the bonds to oxygen around Ni^{3+}, distributed at random in the lattice, is detected by diffraction methods as an average reduction of all the Ni–O distances.

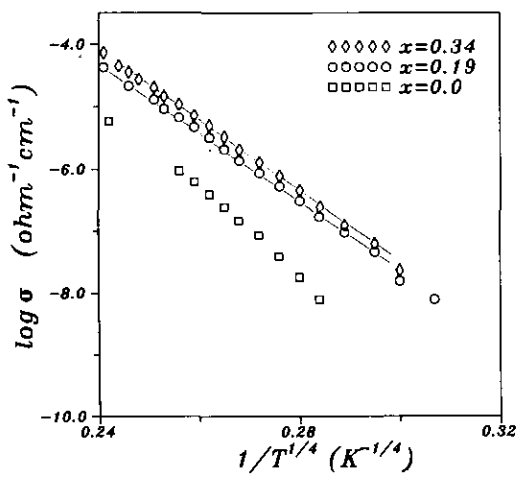

FIG. 5. Electric conductivity vs $T^{-1/4}$ for $Er_{2-x}Ca_xBaNiO_5$.

On the other hand, the absence of strong absorption in the infrared region up to 4000 cm^{-1} (0.5 eV), together with the black color of the samples, which indicates the absorption in the visible region, allows us to estimate an activation energy for hopping higher than 0.13 eV, if we assume that the activation energy is about one-fourth the energy for optical absorption, as observed for some small-polaron solids (24).

The conductivity of the undoped Er_2BaNiO_5 sample, even if it is one order of magnitude smaller than that of the Ca-doped samples, suggests the presence of small amounts of Ni^{3+} cations in the Ni^{2+} sublattice, which gives rise to a similar hopping conduction mechanism. A small percentage of Ba^{2+} or R^{3+} vacancies, due to volatilization losses during the synthesis, are probably in the origin of such effect.

The reduced $R_{2-x}Ca_xBaNiO_{5-\delta}$ samples can also be considered as mixed-valence Ni(I)–Ni(II) compounds. The observed insulating behavior can easily be understood by taking into account that O2 oxygens, involved in the electron hopping conduction mechanism described for the oxidized samples, are partially missing here, which breaks the continuity of the conduction paths along the chains. Ni^+ and Ni^{2+} cations are, therefore, localized and randomly distributed in the structure. The light-greenish color of these compounds is also evidence suggesting the

absence of the intervalence transitions observed in the Ni-oxidized samples.

Compounds in which Ni(I) is stable are very rare. Crespin *et al.* prepared and studied the reduced perovskite $LaNiO_2$ (25), which was the first example of the, later so-called, "parent structure" (17) of the high-T_c superconductors. More recently, reduced samples in the system $La_{2-x}Sr_xNiO_{4-\delta}$ (26–28) have been prepared and characterized. These compounds have a defect structure that can be interpreted as a K_2NiF_4-type structure, in which there are oxygen vacancies in the basal plane, or, alternatively, as a Sr_2CuO_3-type structure with interstitial oxygens. The last example is provided by the compounds of the system $R_4Ni_3O_8$ (R = La, Pr, Nd) (29), showing an intermediate structure between $LaNiO_2$ and T'-Nd_2CuO_4. All of them have been obtained by progressive reduction by hydrogen at relatively low temperatures ($T < 700$ K).

It is worth pointing out the important role played by Ca^{2+} cations in the stabilization of Ni(I) in the reduced $Er_{2-x}Ca_xBaNiO_{5-\delta}$ samples. The treatment with H_2/N_2 of the undoped Er_2BaNiO_5 phase leads to the destruction of the structure by total reduction to metallic Ni. On the contrary, the presence of Ca^{2+}, distributed at random in the Er^{3+} sublattice, allows the reduction to a Ni(I)-containing material, after a first step in which an oxygen-deficient Ni(II) phase can be isolated. Moreover, the maximum Ni(I) content in the reduced phases seems to be equal (or, at least, proportional) to the Ca content; e.g., for R = Er, $x = 0.34$, a mean Ni valence of 1.62(4)+ (which means 38% of Ni(I)) can be reached in the reduced phase $Er_{1.66}Ca_{0.34}BaNiO_{4.64(2)}$.

Similar results are reported for the reduction of lanthanum nickelates (26–28): attempts at reducing La_2NiO_4 lead to La_2O_3 and Ni mixtures, but a lower reduction level can be reached for $La_{2-x}Sr_xNiO_4$, e.g., the composition $LaSrNiO_{3.1}$ can be isolated, maintaining a K_2NiF_4-like structure in which 80% of the total Ni is in the monovalent formal state (27).

The ability of Ca to stabilize a higher oxidation state for Ni is understandable taking into account the more basic character of Ca^{2+} with regard to the rare-earth cation. This is what happens in the oxidized $R_{2-x}Ca_xBaNiO_5$ samples, in which the mean oxidation state of Ni increases regularly with the Ca content. But, surprisingly, the presence of Ca^{2+} seems also to facilitate the reduction processes, by oxygen vacancy creation, that lead to a lowering of the mean oxidation state for Ni. Probably, the oxygen vacancies created in the reduction are better stabilized by the structure when Ca is present. This is in connection with the kind of oxygen that is lost in the reduction process: why are the O2 oxygens and not the O1 preferentially eliminated? A possible explanation can be found in the fact that each O2 is strongly bonded to 2 Ni atoms: these short Ni–O bonds have a larger covalent participation than any other bond to oxygen in the structure. Compared to the O1 oxygens, the O2 are less rich in electron density, i.e., they are more "positively" charged (or less negatively), so they are preferentially chosen during the reduction process. At the same time, structural stresses (7) are partially released with the elimination of these "overbonded" O2 oxygens.

The fact that the maximum number of oxygen vacancies that can be created without destroying the structure equals the number of Ca atoms present in the compound suggests that the O2 oxygen directly bonded to Ca (which are distributed at random in the rare-earth sublattice) are those eliminated in the reduction process, since each Ca (or R) is bonded to only one O2 oxygen. When the corresponding O2 vacancy is formed, the oxygen coordination polyhedron of Ca^{2+} is a 6O1 trigonal prism, which seems to be rather stable. Once all the O2 bonded to Ca are removed, a further reduction leads to the destruction of the structure, in the same way that the reduction of undoped R_2BaNiO_5.

Another question raised is whether the coordination polyhedron of the Ni atoms in the neighborhood of the O2 vacancies is square planar (i.c. = 4) or square pyramidal (i.c. = 5). The first possibility would imply that O2 vacancies are associated by pairs at both sides of Ni. If we accept that each O2 vacancy is coupled to a Ca atom, as shown before, a square pyramidal oxygen coordination for Ni seems to be statistically more realistic: there is no reason why Ca^{2+} should be coupled by pairs in the oxidized samples, taking into account the high synthesis temperatures (1100–1200°C) of these samples, to which a high mixing entropy is associated.

CONCLUSIONS

A Ni(III)–Ni(II) mixed-valence state has been induced by Ca doping in the R_2BaNiO_5 (R = Y, Nd, Er, Lu) phases. The doped samples are black in color, and the electrical conductivity increases with the Ca content. The conductivity is thermally activated due to the presence of local distortions in the lattice that trap the electron holes and hinder the electronic delocalization, which otherwise would lead to metallic behavior. The Ni^{2+}–Ni^{3+} intervalence transitions through O2 oxygen seem to be in the origin of the semiconducting behavior of the samples. These samples can be reduced in two steps. The first one leads to grey oxygen-deficient compounds in which all of the Ni^{3+} cations have been reduced to Ni^{2+}. A further increase of the reduction level can be reached by isothermal heating under a H_2/N_2 flow, which gives rise to greenish Ni(I)–Ni(II) mixed-valence compounds. Even if the overall crystal structure of the reduced $R_{2-x}Ca_xBaNiO_{5-\delta}$ phases remains basically unchanged, the lack of some O2 axial oxygens breaks the continuity of the chains of NiO_6

octahedra, thus hindering the intervalence transitions between Ni^{+}–Ni^{2+}. Both cations are, therefore, localized and distributed at random in the structure. The presence of Ca is essential for the stabilization of the oxygen vacancies and, therefore, for the existence of Ni(I) in the crystal lattice of the reduced samples: the reduction of undoped R_2BaNiO_5 phases leads directly to the destruction of the structure by Ni metal formation.

ACKNOWLEDGMENTS

The authors acknowledge the financial support of the Fundación Domingo Martínez and of the DGICYT to the project PB91-0089. J.B.T. gratefully acknowledges financial support from the Spanish Ministry of Education during his sabbatical. J.A.A. thanks the MDN group at the CEN-Grenoble for their hospitality and the facilities at the Siloé Reactor. The authors thank the ILL for making all facilities available.

REFERENCES

1. S. Schiffler and H. Müller-Buschbaum, *Z. Anorg. Allg. Chem.* **532,** 10 (1986).
2. S. Schiffler and H. Müller-Buschbaum, *Monats. Chem.* **118,** 741 (1987).
3. H. Müller-Buschbaum and Ch. Lang, *J. Less-Common Met.* **142,** L1 (1988).
4. J. Amador, E. Gutiérrez-Puebla, M. A. Monge, I. Rasines, J. A. Campá, J. M. Gómez De Salazar, and C. Ruíz-Valero, *Solid State Ionics* **32/33,** 123 (1989).
5. H. Müller-Buschbaum and P. Sonne, *J. Less-Common Met.* **167,** 185 (1990).
6. H. Müller-Buschbaum and D. Schluter, *J. Less-Common Met.* **166,** L7 (1990).
7. J. A. Alonso, J. Amador, I. Rasines, and J. L. Soubeyroux, *Acta Crystallogr., Sect. C* **47,** 249 (1991); E. García-Matres, J. L. Martínez, J. Rodríguez-Carvajal, J. A. Alonso, A. Salinas-Sánchez, and R. Saez-Puche, *J. Solid State Chem.* **103,** 322 (1993).
8. J. Amador, E. Gutiérrez-Puebla, M. A. Monge, I. Rasines, C. Ruiz-Valero, F. Fernández, R. Saez-Puche, and J. A. Campá, *Phys. Rev. B* **42,** 7918 (1990).
9. J. A. Alonso, J. Amador, J. L. Martínez, I. Rasines, J. Rodríguez-Carvajal, and R. Saez-Puche, *Solid State Commun.* **76,** 467 (1990).
10. A. Salinas-Sanchez, R., Saez-Puche, J. Rodríguez-Carvajal, and J. L. Martínez, *Solid State Commun.* **78,** 481 (1991).
11. E. García-Matres, J. Rodríguez-Carvajal, J. L. Martínez, A. Salinas-Sánchez, R. Saez-Puche, and J. A. Alonso, *Solid State Ionics,* **63–65,** 915 (1993).
12. C. Michel and B. Raveau, *J. Solid State Chem.* **43,** 73 (1982).
13. S. Schiffler and H. Müller-Buschbaum, *Z. Anorg. Allg. Chem.* **540/541,** 243 (1986).
14. H. Müller-Buschbaum and I. Ruter, *Z. Anorg. Allg. Chem.* **572,** 181 (1989).
15. J. B. Goodenough and A. Manthiram, *J. Solid State Chem.* **88,** 115 (1990).
16. J. F. Bringley, S. S. Trail, and B. A. Scott, *Eur. J. Solid State Inorg. Chem.* **18,** 1245 (1991).
17. T. Siegrist, S. M. Zahurac, D. W. Murphy, and R. S. Roth, *Nature* **334,** 231 (1988); M. Azuma, Z. Hiroi, M. Takano, Y. Bando, and Y. Takeda, *Nature* **356,** 775 (1992).
18. H. M. Rietveld, *J. Appl. Crystallogr.* **2,** 65 (1969).
19. J. Rodríguez-Carvajal, "FULLPROF: A Program for Rietveld Refinement and Pattern Matching Analysis," Abstracts of the Satellite Meeting of the XVth Congress of the International Union of Crystallography, p 127. Toulouse, 1990.
20. D. B. Wiles and R. A. Young, *J. Appl. Crystallogr.* **14,** 149 (1981).
21. R. D. Shannon, *Acta Crystallogr., Sect. A* **32,** 751 (1976).
22. J. A. Alonso and I. Rasines, in preparation.
23. A. Salinas-Sánchez, R. Saez-Puche, F. Fernández, A. De Andres, A. E. Lavat, and E. J. Baran, *J. Solid State Chem.* **99,** 63 (1992).
24. P. A. Cox, "The Electronic Structure and Chemistry of Solids." Oxford Univ. Press, 1989.
25. M. Crespin, P. Levitz, and L. Gatineau, *J. Chem. Soc., Faraday Trans. 2* **79,** 1181 (1983).
26. M. Crespin, J. M. Bassat, P. Odier, P. Mouron, and J. Choisnet, *J. Solid State Chem.* **84,** 165 (1990).
27. M. Crespin, C. Landron, P. Odier, J. M. Bassat, P. Mouron, and J. Choisnet, *J. Solid State Chem.* **100,** 281 (1992).
28. M. Medarde, J. Rodríguez-Carvajal, X. Obradors, M. Vallet-Regí, J. M. González-Calbet, and J. Alonso, *Physica B* **180 & 181,** 402 (1992).
29. P. Lacorre, *J. Solid State Chem.* **97,** 495 (1992).